PHYSICAL REVIEW E, VOLUME 63, 025301(R)

Anomalous scaling of velocity and temperature structure functions

R. A. Antonia and R. J. Smalley
Department of Mechanical Engineering, University of Newcastle, New South Wales 2308, Australia
(Received 7 September 2000; published 12 January 2001)

Scaling-range power-law exponents of velocity and temperature structure functions are examined through the dimensional analysis framework of the refined similarity hypotheses using measurements in a variety of turbulent flows and Reynolds numbers. The resulting magnitude of the scaling exponent associated with the locally averaged energy dissipation rate ϵ_r is always larger than 2/3, whereas the exponent for the locally averaged temperature dissipation rate χ_r is always smaller than 2/3. While the ϵ_r exponent may be reconciled with the exponent of the velocity structure function, the distributions of the χ_r and temperature structure function exponents are inherently different.

DOI: 10.1103/PhysRevE.63.025301 PACS number(s): 47.27.Nz, 47.27.Lx, 05.40.−a

In turbulent flows, considerable attention has been devoted to determining the power-law exponents $\zeta_\alpha(n)$ of order n associated with the structure functions $\langle(\delta\alpha)^n\rangle$, viz.,

$$\langle(\delta\alpha)^n\rangle \sim r^{\zeta_\alpha(n)}. \tag{1}$$

Here α represents any of the three velocity fluctuations (u, v, and w) or the temperature fluctuation θ, $\delta\alpha \equiv \alpha(x+r) - \alpha(x)$ is the difference between the values of α at two locations separated by a distance r, and the angular brackets denote time averaging. A major motivation for this has been to establish if the scaling is anomalous, i.e., if the magnitude of $\zeta_\alpha(n)$ departs from $n/3$, the value predicted by Kolmogorov [1], hereafter K41.

Determining $\zeta_\alpha(n)$ is fraught with difficulties, one of which is the identification of a suitable scaling range. There is increasing evidence to indicate that a scaling range which complies with K41 is unlikely to exist at Reynolds numbers usually encountered in laboratory experiments. Even for the atmospheric surface layer, where the Taylor microscale Reynolds number $R_\lambda \equiv \langle u^2\rangle^{1/2}\lambda_u/\nu$, ($\lambda_u \equiv \langle u^2\rangle^{1/2}/\langle(\partial u/\partial x)^2\rangle^{1/2}$) is typically of order 10^4, the local derivatives of $\log\langle(\delta u)^2\rangle$, with respect to $\log r$ [2], do not exhibit plateaux. However, their rate of decrease is sufficiently small over a particular region of r, such that the region may be identified with a scaling range and an average value of ζ_u can be estimated.

In this Rapid Communication, we consider data for $\langle(\delta\alpha)^2\rangle$ obtained in several flows and over a significant range of R_λ. One data set was obtained in the atmospheric surface layer (ASL). The laboratory flows included both shearless (decaying grid turbulence) and sheared flows (free shear flows such as jets and wakes and wall bounded flows). In laboratory flows, fluctuations of temperature, treated as a passive scalar, were measured. The local derivatives of $\langle(\delta\alpha)^2\rangle$ are compared with the K41 predictions for ζ_α and also with those which take into account the intermittency of the energy dissipation rate and scalar dissipation rate fluctuations, via the framework introduced by Kolmogorov [3] in 1962, hereafter K62. When $\alpha = u$, v, or w, the K62 phenomenology (see also [4]) gives

$$\langle(\delta\alpha^*)^2\rangle = C_\alpha\langle x_\alpha^{*2}\rangle, \tag{2}$$

with $x_\alpha \equiv (r\epsilon_r)^{1/3}$, where ϵ_r is the energy dissipation rate, the subscript r denoting averaging over a scale r. C_α is a flow dependent premultiplier, assumed independent of r and ϵ_r. When $\alpha = \theta$ (e.g., [5]),

$$\langle(\delta\theta^*)^2\rangle = C_\theta\langle x_\theta^{*2}\rangle, \tag{3}$$

with $x_\theta \equiv (r^{1/3}\epsilon_r^{-1/6}\chi_r^{1/2})$, where χ_r is the scalar dissipation rate. An asterisk denotes normalization by the Kolmogorov length scale $\eta \equiv \nu^{3/4}/\langle\epsilon\rangle^{1/4}$, Kolmogorov velocity scale $U_K \equiv (\nu\langle\epsilon\rangle)^{1/4}$, and/or Obukhov-Corrsin temperature scale $\theta_K \equiv (\langle\epsilon_\theta\rangle\eta/U_K)^{1/2}$. Using dimensional arguments similar to those of [6], we can also write

$$\langle[(\delta u^*)(\delta\theta^*)^2]^{2/3}\rangle = C_{u\theta}\langle x_{u\theta}^{*\,2}\rangle, \tag{4}$$

with $x_{u\theta} \equiv (r\chi_r)^{1/3}$. We consider here the dependencies of $\langle x_u^{*2}\rangle$, $\langle x_\theta^{*2}\rangle$, and $\langle x_{u\theta}^{*\,2}\rangle$ on both R_λ and flow type. The behavior of these moments is compared with results from K41 and K62. Both K41 and K62 assume that the Reynolds number is very large and that isotropy applies for scales which extend through to the upper end of the scaling range. Complete information about ϵ and χ is not usually available in experiments, reliable statistics associated with these two quantities being more readily accessible via direct numerical simulation (DNS) and the large eddy simulation (LES) data [7,8], albeit only for moderate values of R_λ.

Simultaneous measurements of u and θ were carried out in four types of flow (cylinder wake, circular jet, rough wall boundary layer, and grid turbulence) using hot- and cold-wire anemometry. Only u and v were measured simultaneously in the ASL. For the grid measurements, multiple-wire probes were used. Measurements were made at $x/M = 30$ (M is the mesh grid size) and the R_λ was 52. Details on probe construction may be found in Refs. [9,10]. In all shear flows, in which heat was introduced as a passive scalar, θ was measured with a single cold-wire (Pt-10% Rh wire, diameter $d_w = 0.63$ μm), etched to a nominal length, $l_w \approx 0.7$ mm. These were operated in a constant-current (0.1 mA) anemometer circuit. Measurements in the wake of a heated circular cylinder [11] ($R_\lambda = 230$; diameter $d = 25.4$ mm) were obtained on the axis centreline at $x/d = 70$ using a single hot-wire ($d_w = 2.5$ μm; $l_w \approx 0.6$ mm)

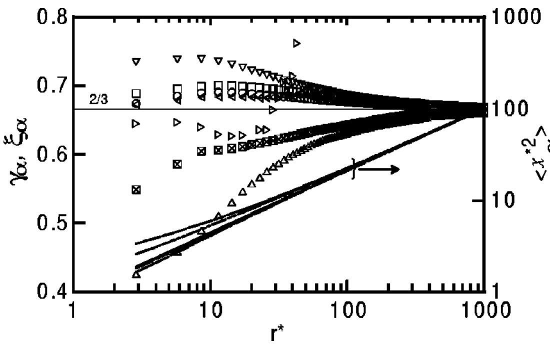

FIG. 1. Distributions in grid turbulence of $\langle x_\alpha^{*2}\rangle$ and the local slopes γ_α and ξ_α, using different approximations for ϵ_f and χ_f. Lines: $\langle x_\alpha^{*2}\rangle$, right ordinate. Symbols: γ_α, ξ_α, left ordinate. $\langle x_u^{*2}\rangle$, γ_u: — - —, $\bigtriangledown$, isotropic approximation to ϵ_f. - - -, $\square$, ϵ_f approximated using Eq. (5). —, $\bigcirc$, 11-term approximation to ϵ_f. $\langle x_\theta^{*2}\rangle$, γ_θ: – –, $\triangle$, isotropic approximations to ϵ_f and χ_f. — - - —, $\boxtimes$, ϵ_f and χ_f approximated using Eqs. (5) and (6) respectively. $\triangleleft$, ξ_u obtained using ESS. $\triangleright$, ξ_θ obtained using ESS.

parallel with the cold-wire. A pair of parallel wires (single hot-wire $d_w = 1.25$ μm and $l_w = 0.26$ mm) was also used for measurements of u and θ on the centreline of a heated circular jet ($R_\lambda = 550$, [12]) at $x/D = 40$ (D is the jet orifice diameter). For the rough-wall turbulent boundary layer ($R_\lambda = 390$; [13], comprising cylindrical rods aligned on a heated wall transverse to the flow), measurements were carried out using an X-wire ($d_w = 1.25$ μm, $l_w/d_w \simeq 200$) in combination with a cold-wire at $y/\delta = 0.37$; δ is the boundary layer thickness. The ASL data ($R_\lambda = 4250$), acquired in an experiment over burnt grassland at a site near Deniliquin, New South Wales, [14], were stored on analog FM tapes and have been recently reanalyzed [15]. The data used here are from a height of 1.7 m above the ground in near-neutral conditions.

Experimentally, approximations to the true (or full) values of the dissipation rates $\epsilon_f \equiv \nu/2(\partial u_i/\partial x_j + \partial u_j/\partial x_i)^2$ and $\chi_f \equiv \kappa(\partial\theta/\partial x_i)^2$ are usually made by assuming isotropy and Taylor's hypothesis, viz., $\epsilon_{iso} \equiv 15\nu(\partial u/\partial x)^2$ and $\chi_{iso} \equiv 3\kappa(\partial\theta/\partial x)^2$. However, in grid turbulence, $\langle\epsilon_f\rangle$ and $\langle\chi_f\rangle$ can be obtained relatively accurately from the streamwise decay rates of the turbulent kinetic energy $\langle k^2\rangle$ and the temperature variance $\langle\theta^2\rangle$. These estimates were compared in [9] with the approximations

$$\epsilon_{ap} = \nu\left[6\left(\frac{\partial u}{\partial x}\right)^2 + 3\left(\frac{\partial u}{\partial y}\right)^2 + 2\left(\frac{\partial v}{\partial x}\right)^2 + 2\left(\frac{\partial u}{\partial y}\right)\left(\frac{\partial v}{\partial x}\right)\right], \tag{5}$$

$$\chi_{ap} = \kappa\left[\left(\frac{\partial\theta}{\partial x}\right)^2 + 2\left(\frac{\partial\theta}{\partial y}\right)^2\right] \tag{6}$$

using data obtained with a six-wire probe. An approximation to ϵ_f, by measuring 11 of the 12 terms using a three-component vorticity probe was also carried out; see Ref. [10]. Although the mean values of ϵ_{ap} and χ_{ap} were in close agreement with $\langle\epsilon_f\rangle$ and $\langle\chi_f\rangle$, this is not a particularly sensitive test for the approximations, since $\langle\epsilon_{iso}\rangle$ and $\langle\chi_{iso}\rangle$ were also in reasonable agreement with $\langle\epsilon_f\rangle$ and $\langle\chi_f\rangle$ in this flow. Other statistics, for example the spectra of ϵ_{ap} and χ_{ap}, were almost identical to those of ϵ_f and χ_f, in severe contrast with ϵ_{iso} and χ_{iso}. It is therefore of interest to consider the effect different approximations have on the distributions of $\langle x_u^{*2}\rangle$ and $\langle x_\theta^{*2}\rangle$, and in particular on the distributions of the scaling exponents

$$\gamma_\alpha = \frac{d(\log\langle x_\alpha^{*2}\rangle)}{d(\log r^*)} \tag{7}$$

for $\alpha = u$ and θ; on the assumption that $\langle x_\alpha^{*2}\rangle \sim r^{*\gamma_\alpha}$. The symbol γ_α is used to allow a distinction with ζ_α, the exponent obtained directly from the structure function, viz.,

$$\zeta_\alpha = \frac{d\log\langle(\delta\alpha^*)^2\rangle}{d(\log r^*)}. \tag{8}$$

Implicit in K62 is the notion that, statistically, δu depends on ϵ_r and C_u is independent of r and ϵ_r. Plateaus in γ_α and ζ_α would be consistent with the existence of a power-law behavior for $\langle(\delta\alpha)^2\rangle$ and a dependence of (δu) on ϵ_r. If γ_α

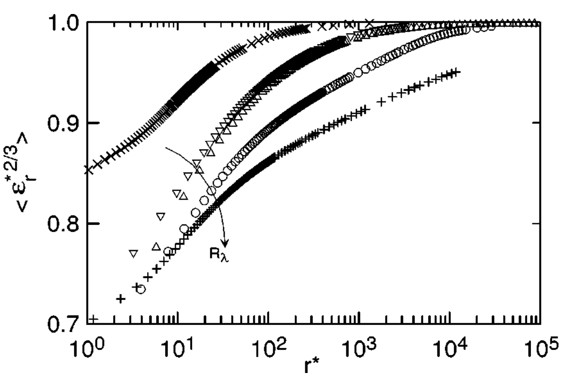

FIG. 2. Distributions of $\langle\epsilon_r^{*2/3}\rangle$ in various flows and different values of R_λ. ϵ approximated using isotropy. $\times$, Grid; $\bigtriangledown$, cylinder wake; $\triangle$, rough wall turbulent boundary layer; $\bigcirc$, circular jet; $+$, ASL.

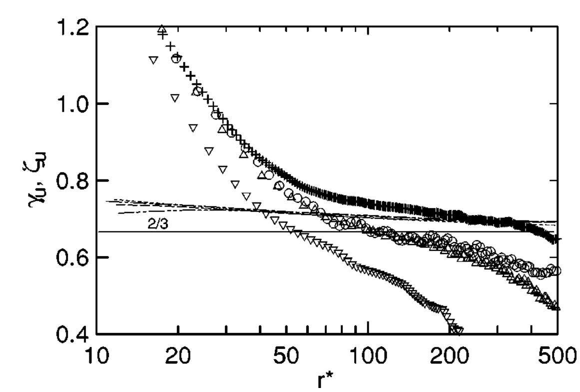

FIG. 3. Scaling exponents γ_u and ζ_u. Lines: γ_u. Symbols: ζ_u. — - —, $\bigtriangledown$, cylinder wake; - - -, $\triangle$, rough wall; – –, $\bigcirc$, circular jet; — - - —, $+$, ASL.

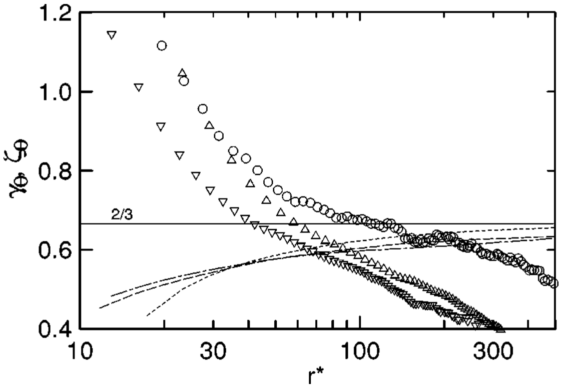

FIG. 4. Scaling exponents γ_θ and ζ_θ. Lines: γ_θ. Symbols: ζ_θ. — - —, ∇, cylinder wake; - - -, $\triangle$, rough wall; – –, $\bigcirc$, circular jet.

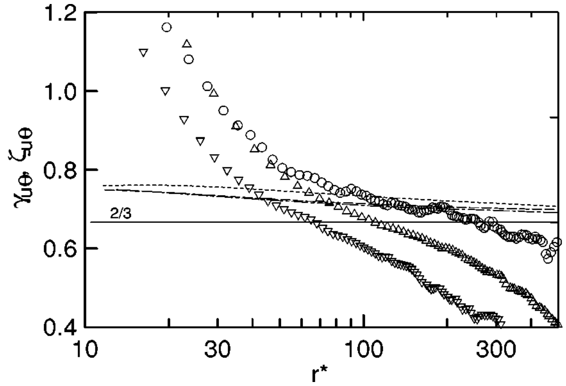

FIG. 5. Scaling exponents $\gamma_{u\theta}$ and $\zeta_{u\theta}$. Lines: $\gamma_{u\theta}$. Symbols: $\zeta_{u\theta}$. — - —, ∇, cylinder wake; - - -, $\triangle$, rough wall; – –, $\bigcirc$, circular jet.

and ζ_α are equal over the same r segment, then C_u is independent of r and ϵ_r. A similar reasoning applies to Eqs. (3) and (4).

The distributions of $\langle x_u^{*2}\rangle$ (Fig. 1) corresponding to the different approximations to ϵ_f exhibit approximately the same behavior (this is also true for $\langle x_{u\theta}^{*2}\rangle$, not shown). The effect on γ_α is unmistakable. The differences in γ_u between different approximations to ϵ_f are primarily confined to $r^* < 100$. The differences are greater for γ_θ, possibly due to the influence of the correlation between ϵ_r and χ_r on $\langle x_\theta^{*2}\rangle$ (see [8]). Relative to the exponents obtained with ϵ_{ap} and χ_{ap}, those obtained with ϵ_{iso} and χ_{iso} depart further from 2/3. Also, for all r^*, the distribution of γ_θ is more ‘‘anomalous’’ than that for γ_u, especially when the isotropic approximations are made. Regardless of the type of approximation, there is an inflection point in γ_α at $r^* \approx 10$, which corresponds roughly with the transition between dissipative and scaling ranges. For the present grid flow, R_λ is too small to expect a scaling range, i.e., a region where ζ_u is constant. The extended-self similarity (ESS) method [16] provides estimates of the scaling exponents ξ_u and ξ_θ, *relative* to $\langle|\delta u|^3\rangle$ and $\langle|\delta u|(\delta\theta)^2\rangle$ respectively. Here, $\xi_u = d\log\langle(\delta u^*)^2\rangle / d\log[\langle|\delta u^*|^3\rangle]$ and $\xi_\theta = d\log\langle(\delta\theta^*)^2\rangle / d\log\langle|\delta u^*|(\delta\theta^*)^2\rangle$. The latter exponents are in reasonable accord with those inferred from $\langle x_u^{*2}\rangle$ and $\langle x_\theta^{*2}\rangle$.

Although the departure from 2/3 for γ_α, obtained from Eq. (7), is overestimated when ϵ_{iso} and χ_{iso} are used (Fig. 1), it is nevertheless of interest to examine how γ_α, estimated using the isotropic approximations, depends on the flow and R_λ, especially since the isotropic approximations are expected to become more reliable as R_λ increases. Figure 2 contains distributions of $\langle \epsilon_r^{*2/3}\rangle$ obtained in different flows and R_λ. When r is sufficiently large, typically of order L, $\langle \epsilon_r^{*2/3}\rangle$ must approach 1 since $\langle \epsilon_r\rangle$ approaches $\langle\epsilon\rangle$. The value of r^* at which this limit is reached must increase as L^* or R_λ increases. Fig. 2 highlights the significant effect R_λ has on $\langle \epsilon_r^{*2/3}\rangle$.

For the flows considered in Figure 2, the corresponding distributions of γ_α and ζ_α, inferred from Eqs. (7) and (8) respectively, are shown in Figs. 3, 4, and 5 for $\alpha = u,\ \theta$, and $u\theta$. While the region for direct comparison can only be within the scaling range, the distribution of γ_u always exceeds 2/3, whereas that for ζ_u only exceeds 2/3 at sufficiently high R_λ. There is a systematic R_λ dependence of ζ_u, consistent with the estimates obtained in other studies [17]. The relatively good agreement in γ_u for different flows tends to suggest that $\langle x_u^{*2}\rangle$ may only apply in the high R_λ limit. The monotonic variation of γ_u, between the inflection near $r^* \simeq 10$ to the limit of about 2/3 at large r^* suggests that, at least when ϵ_f or χ_f are estimated via isotropy, there will not be an unambiguous scaling exponent for $\langle x_u^{*2}\rangle$. Obviously, a proper comparison between ζ_u and γ_u requires an accurate estimate of ϵ_f.

As with Fig. 3, an unambiguous scaling range cannot be discerned in Fig. 4. For $r^* \gtrsim 10$, γ_θ increases with r^*, a trend opposite to that of ζ_θ and also γ_u (Fig. 3); γ_θ is unlikely to exceed 2/3, whereas ζ_θ exceeds 2/3 only at sufficiently high R_λ. The greater discrepancy in γ_θ, relative to γ_u, may be a consequence of the previously observed stronger intermittency of the scalar field relative to the velocity field.

The use of the mixed order structure function $\langle[(\delta\theta)(\delta u)^2]^{2/3}\rangle$, Eq. (4), does not involve the correlation $\langle\epsilon_r\chi_r\rangle$ so that the assumption of isotropy is required only for χ_r. The variation of $\gamma_{u\theta}$ with r^* (Fig. 5) is similar to that of γ_u. This agreement, implying support for the arguments which underpin Eqs. (2) and (4), reflects to some extent the established analogy [11] between the predictions given by K41 and [18].

In summary, the main conclusion which emerges from Figs. 3 to 5 is that the distributions of ζ_u (or $\zeta_{u\theta}$) and γ_u (or $\gamma_{u\theta}$) may be reconcilable at sufficiently large R_λ, whereas those of ζ_θ and γ_θ exhibit inherently different trends with respect to r^*. It would seem that the dimensional argument implicit in Eq. (3) is not as well supported by our measurements than that in either Eq. (2) or Eq. (4). Figure 1 suggests that this inference is unlikely to be strongly affected by the use of the isotropic approximations for ϵ_f and χ_f.

The support of the Australian Research Council is gratefully acknowledged.

[1] A. N. Kolmogorov, Dokl. Akad. Nauk SSSR **32**, 19 (1941).
[2] K. R. Sreenivasan and B. Dhruva, Prog. Theor. Phys. Suppl. **130**, 103 (1998).
[3] A. N. Kolmogorov, J. Fluid Mech. **13**, 82 (1962).
[4] A. M. Obukhov, J. Fluid Mech. **13**, 77 (1962).
[5] N. N. Korchashkin, Izv., Acad. Sci., USSR, Atmos. Oceanic Phys. **6**, 947 (1970).
[6] R. A. Antonia and C. W. Van Atta, J. Fluid Mech. **67**, 273 (1975).
[7] L-P. Wang *et al.*, J. Fluid Mech. **309**, 113 (1996).
[8] L-P. Wang, S. Chen, and. G. Brasseur, J. Fluid Mech. **400**, 163 (1999).
[9] T. Zhou and R. A. Antonia, Phys. Fluids **12**, 35 (2000).
[10] R. A. Antonia, T. Zhou, and Y. Zhu, J. Fluid Mech. **374**, 29 (1998).
[11] R. A. Antonia *et al.*, J. Fluid Mech. **332**, 395 (1997).
[12] G. Xu, R. A. Antonia, and S. Rajagopalan, Europhys. Lett. **49**, 452 (2000).
[13] R. A. Antonia and R. J. Smalley, Phys. Rev. E **62**, 640 (2000).
[14] A. Dyer *et al.*, Boundary-Layer Meteorol. **24**, 181 (1982).
[15] B. R. Pearson, Ph.D. thesis, University of Newcastle, 1999 (unpublished).
[16] R. Benzi *et al.*, Europhys. Lett. **32**, 709 (1995).
[17] B. R. Pearson and R. A. Antonia (unpublished).
[18] A. M. Yaglom, Dokl. Akad. Nauk SSSR **69**, 743 (1949).